Neutron reflectivity studies of field driven transformations in a monolayer of 4-pentadecyl pyridine at Au electrode surfaces

I. Burgess [a], V. Zamlynny [a], G. Szymanski [a], A.L. Schwan [a], R.J. Faragher [a],
J. Lipkowski [a,*], J. Majewski [b], S. Satija [c]

[a] Department of Chemistry and Biochemistry, University of Guelph, Guelph, Ont., Canada, N1G 2W1
[b] MLNSCE, LANSCE-12, Los Alamos National Laboratory, Los Alamos, NM 87545, USA
[c] NIST Center for Neutron Research, NIST, Gaithersburg, MD, USA

Abstract

Neutron reflectometry (NR) has been employed to study the structure and composition of thin films formed by 4-pentadecyl-pyridine (C15-4Py) at a gold electrode surface. The thickness and the water content of films of C15-4Py have been measured as a function of the potential applied to the electrode. At positive potentials, where condensed film is formed, the monolayer contains defects that are filled with water. At very negative potentials, the film is desorbed from the electrode surface. NR has demonstrated that, at these potentials, the amphiphilic molecules remain in close proximity to the gold surface as a thicker and water rich film.
© 2003 Elsevier B.V. All rights reserved.

1. Introduction

Neutron reflectometry (NR) is a relatively new technique that has proved to be very successful in determining the structure of thin organic films deposited either at the air–solution [1–3] or at the solid–solution interface [4,5]. This technique has been shown to be particularly useful in revealing the structure of supported biomimetic membranes [6–12]. At present, there are only a few examples where this technique has been used in conjunction with electrochemistry. Wiesler and Majkrzak [13] and Noel et al. [14–16] employed NR to study the structure of passive oxide films, Hillman et al. to study polymer films at electrodes [17–19] and we have performed neutron reflectivity studies of monolayers and bilayers of surfactants and phospholipids at electrode surfaces [20–23].

The purpose of this paper is to demonstrate the power of in situ NR to reveal previously unknown details of electric-field driven structural transformations of a monolayer of surfactant molecules deposited at a gold electrode. The surfactant used in this study is 4-pentadecyl-pyridine (C15-4Py) which we have studied using electrochemical [24], light scattering [25–27] and in situ infrared reflection absorption spectroscopy (IRRAS) [28] techniques. The differential capacity curves shown in Fig. 1 illustrate the electrochemical behaviour of a monolayer and bilayer films of C15-4Py learned from previous studies. The molecules of C15-4Py form a condensed film at potentials larger than −0.1 V (vs SCE). The capacity of the monolayer in this state is significantly higher than for the bilayer indicating the monolayer film incorporates water. In the potential range between −0.2 and −0.5 V (SCE), the capacity of both the monolayer and the bilayer is higher indicating that the film becomes spongy and incorporates more water. At $E < -0.75$ V (SCE) the capacity of the interface in the presence of the surfactant merges

* Corresponding author. Fax: +1-519-836-2380.
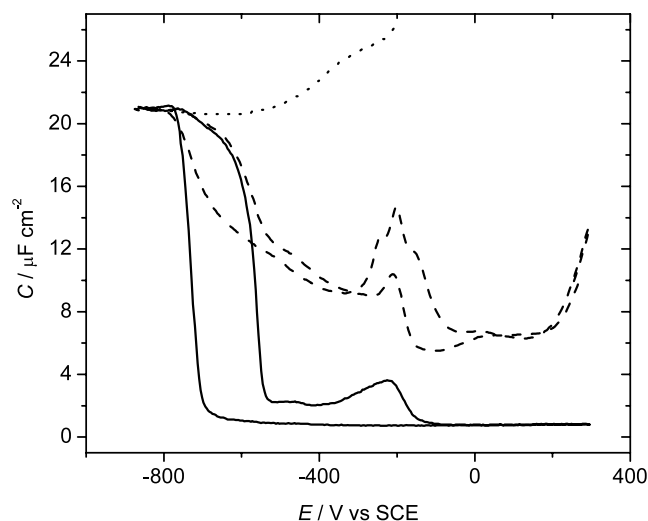E-mail address: lipkowski@chembio.uoguelph.ca (J. Lipkowski).

Fig. 1. Differential capacity of the Au(1 1 1) electrode: dotted line-film represents the film free interface, dashed line represents the interface covered by a monolayer film of C15-4Py molecules deposited at $E = 0$ V (SCE) using the single horizontal touch. The solid line is for a bilayer of C15-4Py. The electrolyte solution was 0.050 M $KClO_4 + 1$ mM $KHCO_3$.

with the capacity of the film-free interface which means that the film is seemingly desorbed from the electrode surface. However, light scattering and fluorescence experiments [25–27] demonstrated that in the desorbed state the surfactant molecules remain close to the electrode surface in the form of aggregates (micelles, flakes or bilayers) and when the direction of the voltage sweep is reversed they spread back onto the metal surface. The formation of aggregates during cathodic desorption of long chain amphiphilic molecules is a general phenomenon that has recently been observed in many laboratories [29–38].

Although the C15-4Py system has been intensely studied, the current understanding is by no means exhaustive. Several issues concerning both the state of the molecules at negative potentials (after being cathodically desorbed) and in the condensed state at more positive potentials remain unanswered. How much water is included in the organic layer in the two states? Are the aggregates formed at negative potentials still attached to the electrode or is there an interstitial layer of water between the organic material and the gold surface? We will demonstrate here that in situ NR can provide precious information on how the water content and the thickness of the film vary with the electrode potential. We will also show that it is a unique technique, which allows one to determine how far the surfactant aggregates are from the electrode surface. The results show how the unique information contributed by NR can lead to a better understanding of the behaviour of surfactant molecules at electrified interfaces.

2. Experimental

2.1. Neutron reflectometry

Neutron reflectivity experiments were carried out on the NG-7 reflectometer at the National Institute of Standards and Technology (NIST) in Gaithersburg, MD. The working electrode was derived from a polished single-crystal (~ 82 mm $\times \sim 38$ mm $\times \sim 13$ mm) quartz substrate obtained from CrysTec GmbH (Berlin, Germany). Thin layers of chromium and gold were sequentially sputtered on the substrates. The resistance of the thin film of gold was on the order of a few ohms. The cyclic voltammetry curves recorded on these thin film gold electrodes resembled CVs recorded at the Au(1 1 1) surface suggesting that the sputtered gold layer was preferentially (1 1 1) oriented. The crystals were degreased with ethanol, irradiated in a UV-cleaner (Jelight, Irvine, CA) for 20 min to oxidize any organic contaminants and then rinsed with Milli-Q water (> 18 MΩ). The irradiation procedure was repeated until the substrate was uniformly hydrophilic. A stream of purified argon was then used to dry the water from the gold surface. The counter electrode was a gold foil of the same approximate surface area as the working electrode. This electrode was cleaned in piranha solution (70:30 mixture of H_2SO_4 and H_2O_2) and thoroughly washed with MilliQ water.

A film of C15-4Py spread at the surface of water in a small Langmuir trough at the equilibrium spreading pressure 33 mN m^{-1} was transferred onto the dry, gold-coated surface of the quartz crystal using the Langmuir–Schaefer technique. We will refer to this procedure as the single touch procedure. A single touch film was characterized by a high capacity, indicating that the film contained a significant amount of water. To improve the film quality, the electrode covered by a monolayer of C15-4Py was detached from the solution at the open circuit potential and brought in contact with the film spread at the air–solution interface for the second time. For small electrodes employed in electrochemical or spectroelectrochemical experiments (surface area ~ 0.25 cm^2), a bilayer was formed using the double touch method. For the large electrodes (surface area ~ 30 cm^2), used in neutron reflectivity experiments, we were only able to transfer a monolayer film by the double touch method.

The working and the counter electrodes were then assembled into a special cell made of Teflon, which was also cleaned in the piranha solution. The electrolyte solution was 50 mM NaF prepared in either MilliQ H_2O, D_2O (99.9%) from Sigma (St. Louis, MO), or a mixture of H_2O and D_2O. The electrolyte solution was degassed with argon and then introduced into the inlet of the Teflon cell. The reference electrode (Ag/AgCl,

$E \sim -40$ mV vs SCE) was then placed in an arm leading into the Teflon block.

Neutron reflectivity measures the normalized (by the incident flux) intensity of specularly reflected neutrons as a function of the momentum transfer vector Q_z. A fixed neutron wavelength of 4.76 Å was used. The error points on the data represent the statistical errors in the measurements (standard deviation σ). A constant instrumental resolution of $\Delta Q_z/Q_z = 0.043$ (FWHM) was used throughout the scan. An 'inverted' geometry, in which the gold-coated quartz electrode was above the solvent phase, was used in our experiments. Varying the angle of incidence allowed reflectivities to be measured in the Q_z range of ~ 0.0 to up to 0.18 Å^{-1}. Reflectivities with reasonable statistics were measured down to values of $R \sim 3 \times 10^{-6}$. Typical counting times were 8–10 h, excluding background measurements. The data were reduced taking into account the neutron beam transmission through the quartz substrate and corrected for the background. Determination of the background was made by deliberately misaligning the crystal so that the non-specular reflection was measured on both sides of the specular angle. The averaged off-specular signal was then subtracted from the measured specular curve. This procedure was performed for each system studied. To illustrate the background correction procedure, Fig. 2 shows a representative reflectivity curve, the two background curves and the background-corrected curve. The scattering length density (SLD) and the film thickness data were determined by fitting a model to the reflectivity curve using the PARRATT 32 fitting algorithm [39] and MLAYER algorithm developed at NIST. Uncertainties for the best fit SLD and thickness values were calculated from the experimental errors using the method described in [40].

NR data of the crystals in air were used to characterize the thickness, SLD and roughness of the chromium and gold layers. These parameters were used as starting parameters for the subsequent fitting involving the surfactant monolayers.

2.2. Synthesis of deuterated C15-4Py
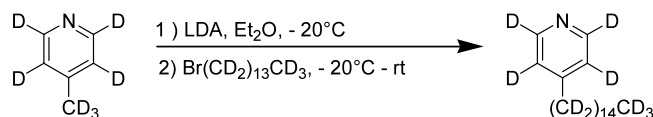
The procedure was altered from the previous synthesis of 4-pentadecylpyridine [24]. To a flame dried 25-ml round bottom flask was added 4-picoline-d_7 (1.04 mmol, 104 mg, 100 µl, C–D–N isotopes, 98.7%D) and dry Et$_2$O (5 ml) and the mixture was cooled to -20 °C. LDA (1.05 eq, 1.09 mmol, 1.5 M, 0.73 ml) was added dropwise and the solution was stirred for 1.5 h. Neat 1-bromotetradecane-d_{29} (1.00 eq, 1.04 mmol, 316 mg, C–D–N isotopes, 98.3%D) was added and stirring continued for an additional hour. The cold bath was removed and the mixture was stirred overnight, diluted with Et$_2$O (15 ml) and filtered. The Et$_2$O filtrate was washed with water (5×20 ml), brine (20 ml) and dried over Na$_2$SO$_4$. The solvent was removed in *vacuo*
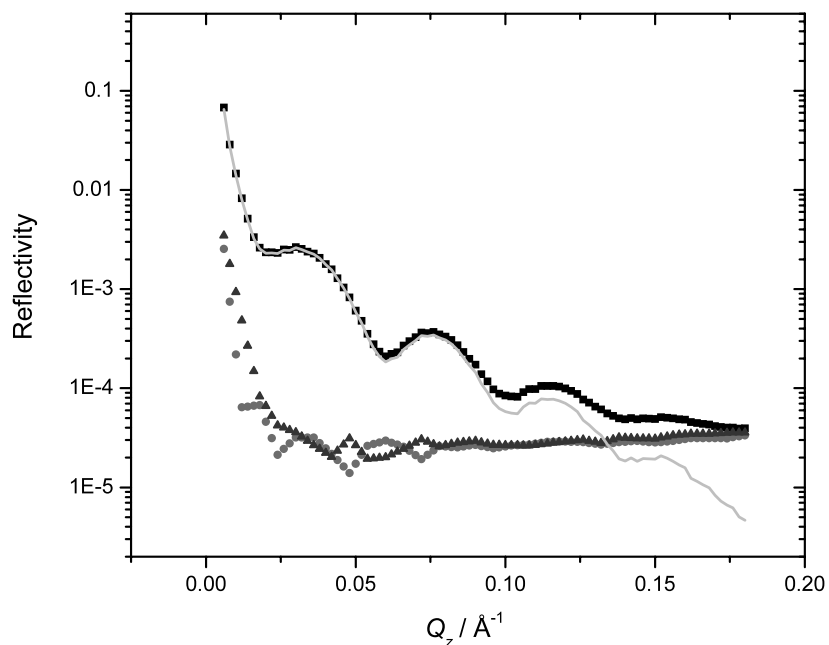

Fig. 2. The influence of the background correction on the specular reflectivity data is shown. The uncorrected specular data are shown by the square data points, while the triangles and circles show the background reflectivity determined with the two off-specular measurements. The solid line is the result of subtracting the averaged, off-specular data from the specular measurements.

yielding 4-pentadecylpyridine-d_{35} (210 mg, 62%, 94.7% pure (GC determination)) as an oil. The product was chromatographed twice (silica gel, flash conditions, (15% EtOAc/hexanes)) to yield 4-pentadecylpyridine-d_{35} as a pale yellow oil, 166 mg (49%), 98.9% purity (GC), mp 19.5–20.5 °C.

2.3. Spectroscopic data

^{2}H-NMR (61 MHz, CDCl$_3$), δ: 8.50 (br s, 2H), 7.12 (br s, 2H), 2.53 (br s, 2H), 1.54 (br s, 2H), 1.17 (br s, 24H), 0.81 (br s, 3H).

^{13}C {^{2}H broadband decoupled} (150 MHz, CDCl$_3$), δ: 151.4, 149.1, 123.3, 34.1, 30.4, 29.0, 28.3 (br, intense), 28.1, 28.0, 27.8, 21.3, 12.8.

IR (neat): ν 2197 (C–D), 2095 (C–D), 1567, 1558, 1536, 1301, 1087, 970 cm^{-1}.

MS (EI), m/z (%): 324 ((M)$^+$, 27), 275 (21), 114 (73), 86 (67), 84 (100).

Elemental Analysis for C$_{20}$D$_{35}$N Calc: C 74.03, D/as H 10.80, N 4.32%. Found: C 73.98, D/as H 10.49, N 4.17%.

2.4. Background and methodology

Since this paper is addressed to electrochemists less familiar with NR, we will give some background that should help the interpretation of the neutron reflectivity data presented in the following section. The reflection of neutrons is well understood and there are a number of reviews that provide a rigorous treatment of the theoretical foundations of this technique [41–46]. The specular reflection of neutrons from an interface consisting of multiple parallel phases is described by the same law as the reflection of an electromagnetic wave polarized in the direction normal to the plane of incidence. The reflection of neutrons from a multilaminar interface can be calculated in an analogous fashion to the optical matrix method for electromagnetic radiation described by Hansen [47], or equivalently by Parratt's recursion method [39], provided the SLD (see below), roughness and thickness of each layer are known.

For neutrons, the refractive index of a given phase may be calculated from the knowledge of SLD ρ using the formula:

$$n^2 = 1 - (\lambda^2/\pi)\rho \tag{1}$$

where λ is the neutron wavelength. The dependence of the SLD on the composition of a given phase is described by the formula:

$$\rho = \sum_j b_j n_j \tag{2}$$

where b_j is the scattering length and n_j is the number density of atomic species j. The neutron scattering length is determined empirically and the value for various elements and their isotopes are tabulated [48]. The isotopic variation in scattering length leads to an intrinsic advantage of neutron reflectivity over similar techniques employing electromagnetic radiation such as X-ray reflectivity and surface plasmon resonance. As different isotopes have differing scattering lengths one can probe specific parts of a system by introducing controlled isotopic variation.

When the SLD profile of an interface is known, a matrix method or a recursion method is usually used to calculate reflectivity curves. However, for pedagogical reasons the relation between the reflectivity and the structure of the interface is better revealed by the analytical expressions derived with the help of the kinematic approximation [49]. The kinematic approximation has been shown to describe the reflection of neutrons from stratified media very well when the reflectivity is significantly less than unity. In the simplest case, when a film of ρ_1 and thickness τ_1 is sandwiched between two phases of identical SLD ρ, the expression for the reflectivity is given by [42]:

$$R = \frac{16\pi^2}{Q_z^4}\left[4(\rho_1 - \rho)^2 \sin^2\left(\frac{Q_z\tau}{2}\right)\right] \tag{3}$$

where the reflectivity is proportional to the square of the difference between the SLD of the film and the backing and fronting phases and inversely proportional to the fourth power of the momentum transfer vector. While in spectroelectrochemical studies, the reflectivity of photons is frequently plotted as a function of the angle of incidence (θ), Eq. (3) shows that in the case of neutrons it is convenient to plot the data as a function of the momentum transfer vector Q_z (where $Q_z = 4\pi \sin \theta / \lambda$).

In our case, the reflection of neutrons took place at an interface consisting of five parallel phases as schematically shown in Fig. 3. Table 1 lists the numerical values of the scattering length densities of the materials used in
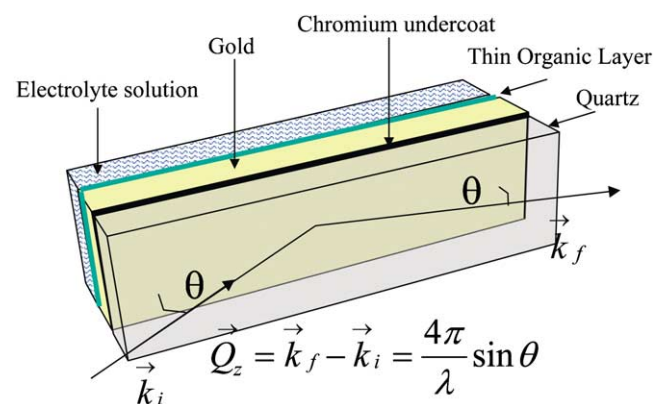

Fig. 3. Schematic representation of the interface consisting of five parallel phases employed in our studies.

Table 1
Calculated SLD values for the materials used in this study

Material/substance	$\rho \times 10^6/\text{Å}^{-2}$
Quartz	4.18
Chromium	3.03
Gold	4.50
$-CH_2-$	-0.49 (determined for $C_{10}H_{22}$)
$-CD_2-$	6.60 (determined for $C_{10}D_{22}$)
D_2O	6.37
H_2O	-0.56

this study. Each phase contributes to the measured neutron reflectivity and to understand the shape of the experimental reflectivity curves presented in the next section, it is instructive to examine the contribution of the individual lamina. To do this we have used the recursion scheme for stratified media described by Parratt [39] to calculate the reflectivity of a simulated interface. These calculated reflectivities are then compared to the reflectivities predicted by the kinematic approximation.

We start by first looking at a 20 Å thick film of hydrogenated surfactant deposited on gold. To simplify the analysis a mixed D_2O/H_2O solvent is simulated such that the SLD for the solvent is contrast matched to the gold (gold contrast matched water or GCMW). We also temporarily neglect the presence of the quartz (SiO_2) and the thin film of Cr. Curve 1 of panel A in Fig. 4 plots the SLD profile in the direction normal to the interface. The reflectivity curve calculated for this profile is presented in panel B and shows the reflectivity decreases quickly with Q_z. This decay is modulated by the interference between neutrons reflected from the front and the back sides of the organic film lamina. In panel C the same set of data is plotted as $Q_z^2\sqrt{R}/8\pi$ against Q_z. This presentation eliminates the Q_z^{-4} dependence of the reflectivity and allows a better analysis of the interference fringes. Consistent with Eq. (3), the period of the oscillation is equal to $\Delta Q_z = 2\pi/\tau_1$ which gives the thickness of the film τ_1. Also the amplitude of the oscillation gives the absolute value of the difference between SLDs $|\rho_1 - \rho|$, from which information on the composition of the film can be determined, with the help of Eq. (2).

Fig. 4. (a) Calculated SLD profiles for components of the interface shown in Fig. 2, assuming that the SLD for the solution phase is contrast matched to gold. Blue ribbon (curve 1), hydrogenated film with a solvent contrast matched to gold, chromium and quartz neglected; red ribbon (curve 2), chromium layer, solvent contrast matched to gold without organic film; green ribbon (curve 3), SLD profile with chromium and a film of hydrogenated species. (b) Reflectivity curves calculated from the SLD profiles in Fig. 2a. (c) Plot of $Q_z^2\sqrt{R}/8\pi$ vs Q_z calculated from the reflectivity curves shown in Fig. 2b.
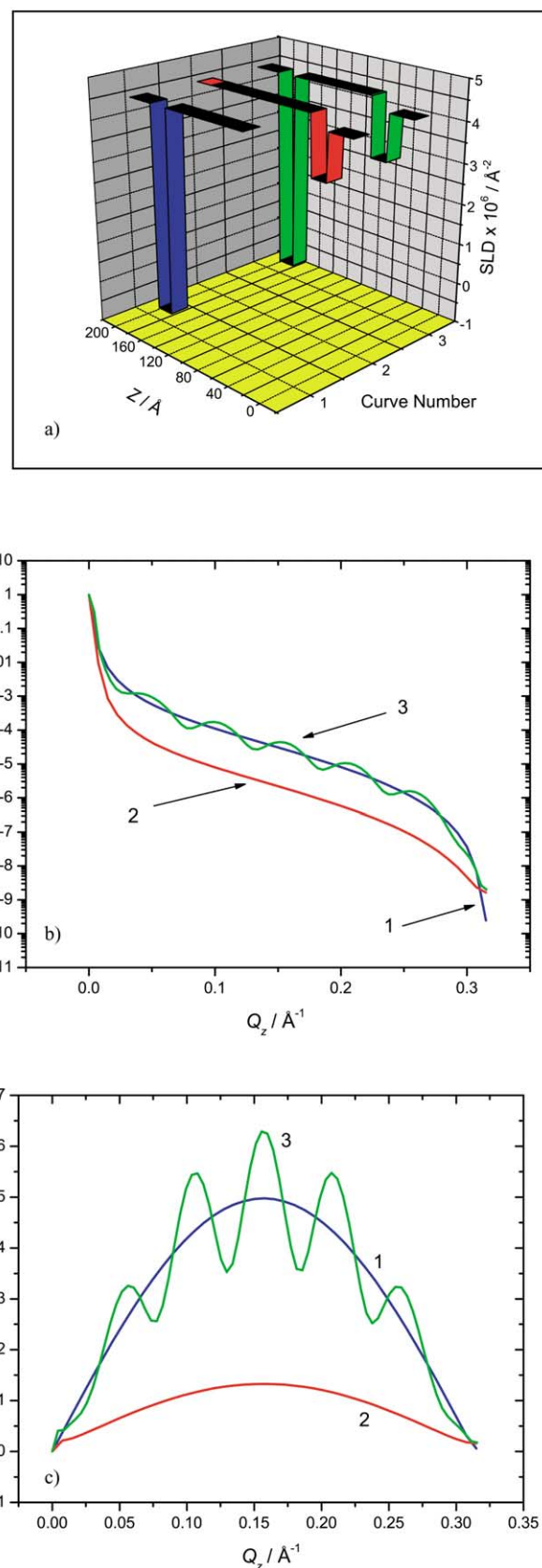
Fig. 4

We now turn our attention to the role of the chromium layer. A chromium layer has to be present in order to ensure adhesion of the gold to the quartz. Curve 2 in Fig. 4a plots the SLD profile for an interface that consists of quartz, 20 Å Cr, gold and gold matched solvent in the absence of the film. The SLD contrast between Cr and either adjacent layer (gold and quartz have very similar SLDs) is very weak and as Fig. 4b shows the reflectivity is much lower in this case. The effect of the SLD contrast on the amplitude can be conveniently seen when the data are plotted as $Q_z^2\sqrt{R}/8\pi$ in Fig. 4c. Curves 1 and 2 in Fig. 4c have the same periodicity (because they have the same thickness). However, curve 2 has much lower amplitude consistent with the much lower contrast shown in the SLD profile in Fig. 4a.

Finally, we place the film of organic molecules on a 100 Å thick gold film sputtered on top of the Cr layer. The SLD profile at the interface is now represented by curve 3 in Fig. 4a. The reflectivity curve corresponding to this profile shows a new interference fringe pattern with higher frequency due to the thick gold layer. Now when the gold is sandwiched between the chromium layer and the organic film its presence becomes visible. Curve 3 in Fig. 4c demonstrates that this pattern results from a sum of two periodic functions. A low frequency component whose periodicity is determined by the thickness of the organic film and to a lesser extent from the chromium, which has the same thickness but a much lower amplitude, and a high frequency component determined by the thickness of the gold film.

The preceding discussion reveals how neutron reflectivity can be used to provide direct information concerning both the thickness and the composition via the SLD of the various layers in the interface. This constitutes an advantage over ellipsometry or surface plasmon resonance methods where the value of the refractive index (composition) of the film is usually assumed in order to determine its thickness. However, in order to directly determine these quantities the reflectivity has to be measured in a sufficiently large range of Q_z so that at least one half of the longest period interference fringe, corresponding to the thinnest layer in the interface, is observed on the reflectivity curve. In fact, the spatial resolution for a film of thickness τ is defined as $\tau = \pi/Q_{z,max}$ where $Q_{z,max}$ is the maximum momentum transfer vector accessible to the experiment [41].

The NG7 line at the NIST Center for Neutron Research (NCNR) allows one to measure reflectivity up to $Q_{z,max} = 0.25$ Å^{-1}. At the NG1 reflectometer at the NCNR, experiments can be run routinely up to 0.3 Å^{-1} [9,11] and in an exceptionally well-designed experiment even up to 0.7 Å^{-1} [12]. For $Q_{z,max} = 0.25$ Å^{-1}, the spatial resolution is ~ 12 Å and for $Q_{z,max} = 0.15$ Å^{-1} it is ~ 20 Å. This resolution is sufficient to study polymer films or corrosive layers with the thickness on the order of 100 Å. However, it imposes a limitation on studies of monolayers and bilayers of surfactants and phospholipids where the thickness of the adsorbed film is comparable to the spatial resolution.

The common procedure used to calculate the SLD profile from the reflectivity curve is to guess the profile, calculate the theoretical reflectivity curve using the optical matrix or recursion method and to compare the calculated and the observed curves. A least squares iterative procedure is then used to vary the parameters of the SLD profile until a good fit between the calculated curve and the experimental data is achieved. Although, the inversion of the reflectivity data is not unique and the SLD profile calculated from the reflectivity curve is not the only mathematical function that fits the reflectivity curve, it usually gives a good physical model of the interface. In order to reduce the ambiguity and the potential non-uniqueness of the fitting procedure, one can employ several different contrasts whereby the experiment is performed using different isotopic profiles. In our experiments we studied a hydrogenated layer of C15-4Py against a mixture of H_2O and D_2O with an SLD matched to that of gold (GCMW). The other contrasts studied consisted of a hydrogenated organic film against a solvent composed of D_2O and an inverted contrast, consisting of a deuterated C15-4Py (d-C15Py) film measured against an H_2O backing.

To further reduce the number of adjustable parameters it is critical to determine a portion of the structural information from an independent experiment. In our case, the thickness, roughness and the SLD of chromium and gold layers sputtered onto the quartz crystals were determined independently by measuring the neutron reflectivity of the crystals in air. Typical neutron reflectivity data for one of the crystals in air is shown in Fig. 5. The solid line is the least-square fit to the data and the resulting SLD profile is shown in the inset. The fit parameters for all the crystals studied are summarized in Table 2. The SLD for Cr and Au layers are slightly higher than the values calculated for the bulk phases. For Cr, slightly higher SLDs may indicate an admixture of Au atoms that occurred during the sputtering. Therefore, for crystal A the fit was done assuming that the chromium layer can be divided into pure Cr and intermediate Cr/Au laminae. One chromium layer was sufficient to fit the data for crystals B and C. Two fitting procedures were employed to calculate the SLD profile for the film-covered electrode. (1) The SLD, thickness and roughness of the gold and chromium layers were assumed to be constant and equal to the values determined for the crystals in air. In addition, the roughness of the organic layer was assumed to be equal to the roughness of the gold layer. In this procedure, the only adjustable parameters were
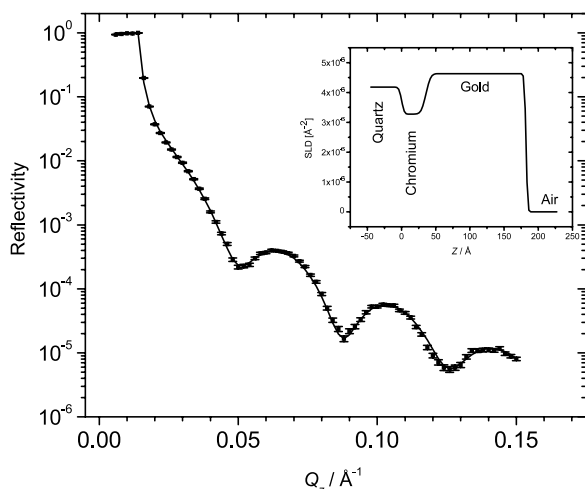
Fig. 5. Representative neutron reflectivity curve measured in air for one of the Au/Cr modified quartz substrates used in the neutron reflectivity studies.

the thickness and the SLD of the organic film. (2) The SLD and the thickness of the organic layer determined from the first fitting procedure and the data for chromium and gold layers determined for the crystals in air were used as initial values of a multi-parameter fit in which for each phase all parameters were allowed to vary to reach the minimum of the χ^2 function. With the exception of one case that will be discussed below the differences between the fit parameters for the organic film obtained by the two procedures were small.

3. Results

We have performed separate experiments on monolayers of C15-4Py involving three different contrasts. In each case, we measured the reflectivity profile at two potentials, one corresponding to the capacitive minimum and the other sufficiently negative to cathodically desorb the insoluble monolayer.

We start our discussion with a hydrogenated C15-4Py film and GCMW-based electrolyte. These experiments were performed on crystal 'C' where the SLD of the gold layer was determined from the neutron in air experiments to be 4.52×10^{-6} Å^{-2} (see Table 2). The exact

SLD of the GCMW solvent was determined by measuring the reflectivity curve for the GCMW against a silicon block. The experimentally determined SLD for the GCMW was 4.50×10^{-6} Å^{-2}. Fig. 6 plots the data obtained from the reflectometry experiments as $Q_z^2\sqrt{R}/8\pi$ vs Q_z. Curve 1 in Fig. 6 corresponds to the run at $E = 100$ mV and is qualitatively very similar to curve 3 in Fig. 4c. There is a high frequency oscillation superimposed on a lower frequency signal having maximum amplitude of roughly 4×10^{-6} Å^{-2} at $Q_z \approx 0.12$ Å^{-1}. As the solvent phase has been contrast matched to the fronting layer (gold), Eq. (4) can be used to estimate the thickness and SLD of the layer between the solvent and gold. Doing so for curve 1 in Fig. 6 gives an approximate SLD and thickness for this layer of 0.5×10^{-6} Å^{-2} and 26 Å, respectively. The low frequency signal of curve 2 in Fig. 6 has smaller amplitude ($\sim 2.8 \times 10^{-6}$ Å^{-2} at a maximum $Q_z \approx 0.1$ Å^{-1}) and the period of its low frequency signal has been shortened. This is indicative of a thicker film with lower contrast compared to curve 1 and indeed, using Eq. (4) one determines a thickness of 32 Å and an SLD of $1.3 \times$
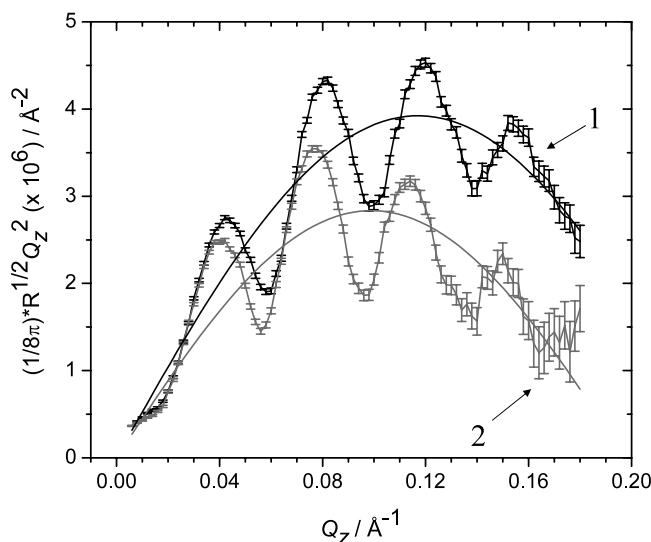

Fig. 6. The experimental NR data obtained for the hydrogenated C15-4Py film measured in GCMW based electrolyte at 100 mV (curve 1) and −800 mV (curve 2) plotted as $Q_z^2\sqrt{R}/8\pi$ vs Q_z. The solid lines are drawn as a 'guide to the eye' to emphasise the low-frequency component in the overall reflectivity signal.

Table 2
Fitting analysis results for the NR of the crystals measured in air

Crystal	Cr layer			Au/Cr layer			Au layer			χ^2
	10^6 SLD/Å^{-2}	τ/Å	σ/Å	10^6 SLD/Å^{-2}	τ/Å	σ/Å	10^6 SLD/Å^{-2}	τ/Å	σ/Å	
A	3.27 (±0.08)	20.7 (±0.8)	4.5	3.82 (±0.06)	8.9 (±1.0)	4.5	4.67 (±0.04)	74.4 (±0.5)	4.5	1.8
B	3.28 (±0.06)	35.5 (±1.2)	3.1	N/A	N/A	N/A	4.63 (±0.03)	146.3 (±0.8)	5.4	3.7
C	3.22 (±0.08)	36.1 (±1.5)	3.0	N/A	N/A	N/A	4.52 (±0.04)	131.0 (±1.0)	5.4	3.1

Roughness in Å. $\chi^2 = 1/(N-v)\Sigma_{i=1}^{N}[(R_{cal} - R_{meas})/\sigma_{meas}]^2$ where N, number of experimental points; v, number of adjustable parameters; σ_{meas}, standard deviation for a given reflectivity point R_{cal}.

10^{-6} Å^{-2}. These numbers can only be considered approximate values because the contribution of the chromium layer to the overall reflectivity curve has been neglected. Nevertheless, because of the poor contrast between the Cr and its adjacent laminae (quartz and gold) the Cr layer has only a relatively small contribution to the reflectivity. Therefore, the values determined for the adsorbed layer via Fig. 6 and Eq. (4) provide excellent starting values to be used in the fitting procedure.

Fig. 7a shows the results of the fitting analyses based on Parratt's algorithm for the reflectivity measurements in GCMW at 100 mV. The points with error bars are the experimentally measured data while the solid lines represent the reflectivity curve calculated from the best-fit model. The SLD profiles corresponding to the best-fit model of the interface are depicted in the insets.
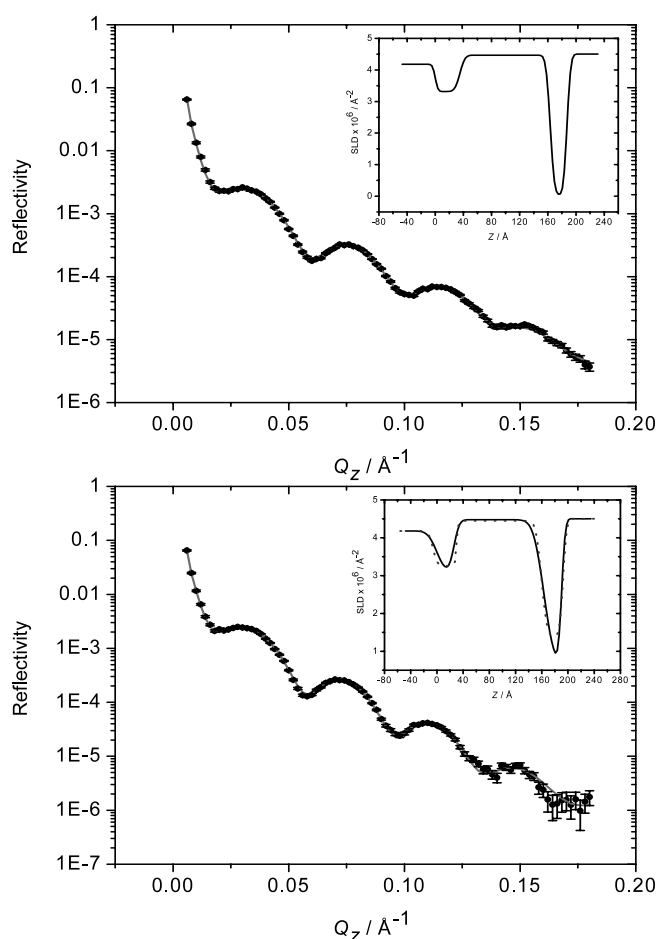

Fig. 7. Experimentally determined reflectivity curves (points with associated error bars) and calculated reflectivity curves (solid lines) from the best-fit modelling of hydrogenated C15-4Py (h-C15Py) measured against 50 mM NaF in GCMW. Panel A shows the data when the working electrode potential was 100 mV vs SCE and panel B for the measurement at $E = -800$ mV vs SCE. Insets to both panels provide the SLD profile of the interface in the direction perpendicular to the surface; solid line for the fit with variable parameters of Cr and Au layers; dotted line with fixed parameters of Cr and Au layers.

The first fitting procedure (with fixed parameters for Cr and Au layers) gives values for the thickness and SLD of the h-C15Py layer at 100 mV equal to 23.2 ± 1.0 Å and $(0.02 \pm 0.15) \times 10^{-6}$ Å^{-2}, respectively. When the thickness and SLD of the Cr and Au layers are allowed to float (procedure 2) the fit parameters for the organic film are 22.6 ± 1.0 Å and $(-0.31 \pm 0.15) \times 10^{-6}$ Å^{-2}. The differences between the results of the two fitting procedures are within the experimental errors. The film thickness determined from the fit is only 10% smaller than the thickness approximated using Eq. (3). Again, the SLD of the surfactant layer determined from the fit agrees favourably with the results predicted from the analysis above. The fit parameters obtained by procedure 2 are compiled in Table 3.

The SLD value of the layer can be used to estimate the volume fraction, (x), of solvent present in the thin organic film if one assumes that the layer consists of only alkyl tails and solvent.

$$\rho_{total} = x\rho_{solvent} + (1-x)\rho_{org} \qquad (4)$$

The value of $\rho_{solvent}$ is known (4.50×10^{-6} Å^{-2}) while the SLD of the film of a hydrocarbon molecules can be determined from the density of *n*-alkanes to be -0.49×10^{-6} Å^{-2}. Using Eq. (4), the volume percent of solvent in the film is determined to be (10 ± 3)% at 100 mV.

For $E = -800$ mV vs SCE, the reflectivity curve and the best fit to the data are shown in Fig. 7b. Solid line in the inset to Fig. 7b plots the SLD profile, when the experimental data are fit using fixed parameters of Cr and Au layers. The best fit model reveals a 32.8 ± 1.8 Å film with an SLD of $(1.45 \pm 0.26) \times 10^{-6}$ Å^{-2}. Again, the results of the fitting procedure are in good agreement with those predicted by Eq. (3). With the help of Eq. (4) the volume percent of solvent in the film at -800 mV is estimated to be (39 ± 5)%. Apparently, when the potential of the working electrode is changed from 100 to -800 mV vs SCE, the organic film swells, becomes rich in water, but remains in a close proximity to the electrode surface. Table 3 shows that when the parameters of the chromium and gold layers are allowed to float the best fit gives a thinner film with lower SLD and a significantly larger roughness. The dotted line in the inset to Fig. 7b shows that when the thickness is convoluted with the roughness the resulting SLD profile is not too different from the profile determined from the first fitting procedure. The new fit gives a somewhat lower SLD of the organic film. Such behaviour suggests that the surfactant molecules may be concentrated in the middle of the film with the portion of the film adjacent to the metal being rich in water.

In an effort to further verify the validity of our data, we repeated the neutron reflectivity measurements using two additional contrasts. In Fig. 8 we present experimental reflectometry data, the reflectivity calculated from the best-fit modelling and the SLD profile normal

Table 3
Fitting analysis results for the NR of the C15-4Py film-modified crystals measured as a function of potential

System	Chromium			Gold			Organic			χ^2
	τ [a]	SLD [b]	σ [c]	τ [a]	SLD [b]	σ [c]	τ [a]	SLD [b]	σ [c]	
GCMW $E = 100$ mV	32.6 (±1.6)	3.24 (±0.06)	6.3 (±1.3)	131.1 (±1.0)	4.48 (±0.01)	6.4 (±1.0)	22.6 (±1.0)	−0.31 (±0.16)	6.4 (±0.6)	2.1
GCMW $E = -800$ mV	26 (±5.0)	3.06 (±0.02)	11.0 (±2.1)	137.3 (±1.5)	4.48 (±0.01)	6.5 (±1.5)	27.1 (±1.0)	0.57 (±0.09)	12.7 (±0.4)	1.2
dC15Py $E = 100$ mV	31.5 (±2.4)	2.86 (±0.11)	11.8 (±1.0)	151.7 (±3.1)	4.18 (±0.01)	8.4 (±0.8)	18.0 (±3.0)	5.65 (±0.38)	3.9 (±3.9)	4.9
dC15Py $E = -800$ mV	24.1 (±1.0)	2.64 (±0.05)	4.8 (±1.1)	157.9 (±0.7)	4.18 (±0.01)	3.27 (±0.5)	33.7 (±2.0)	2.15 (±0.03)	6.6 (±0.8)	9.7
hC15Py $E = 100$ mV	27.5 (±1.1)	3.28 (±0.03)	7.1 (±2.1)	78.4 (±0.4)	4.54 (±0.01)	3.9 (±1.0)	25.0 (±2.0)	0.87 (±0.03)	4.3 (±0.4)	8.2
hC15Py $E = -800$ mV	16.5 (±5.5)	3.06 (±0.04)	3.3 (±0.4)	81.9 (±1.5)	4.60 (±0.01)	3.6 (±0.5)	41.5 (±2.0)	3.76 (±0.03)	5.1 (±2.1)	5.8
hC15Py $E = -300$ mV	31.9 (±2.0)	3.21 (±0.07)	3.6 (±0.9)	78.73 (±0.9)	4.58 (±0.01)	6.833 (±1.2)	23.29 (±1.5)	1.97 (±0.2)	3.6 (±2.2)	3.3

$\chi^2 = 1/(N-v)\sum_{i=1}^{N}[(R_{cal} - R_{meas})/\sigma_{meas}]^2$ where N, number of experimental points; v, number of adjustable parameters; σ_{meas}, standard deviation for a given reflectivity point R_{cal}.
[a] Thickness of layer in Å.
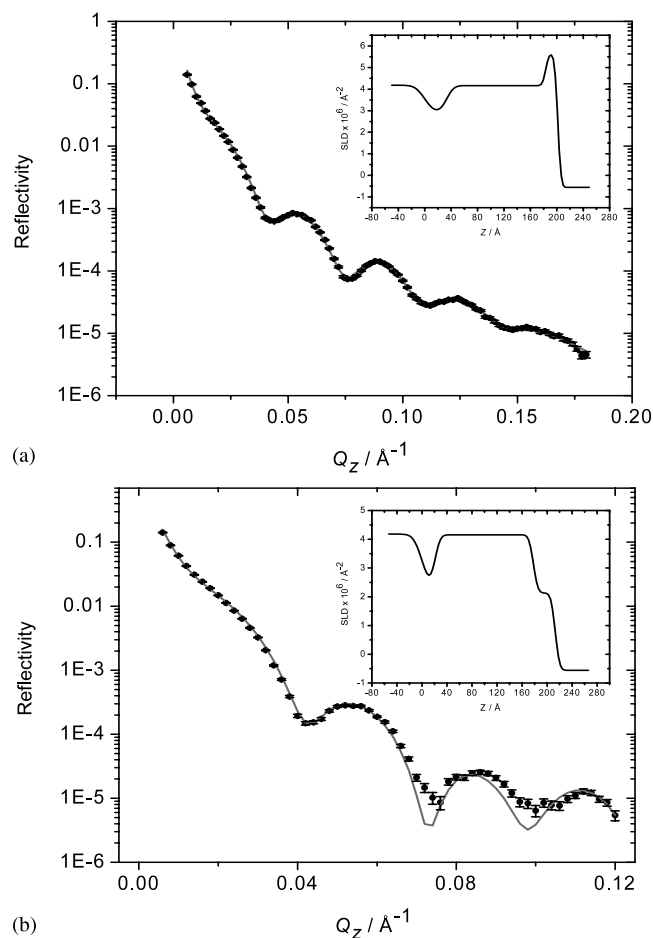[b] SLD × 10^6 Å^{-2}.
[c] Roughness in Å.

Fig. 8. Experimentally determined reflectivity curves (points with associated error bars) and calculated reflectivity curves (solid lines) from the best-fit modelling of d-C15Py measured against 50 mM NaF in H_2O. Panel A shows the data when the working electrode potential was 100 mV vs SCE and panel B for the measurement at $E = -800$ mV vs SCE. Insets to both panels provide the SLD profile of the interface in the direction perpendicular to the surface.

to the interface for the d-C15Py in H_2O based electrolyte contrast. Measurements were performed on crystal 'B' at $E = 100$ mV vs SCE (Fig. 8a) and $E = -800$ mV vs SCE (Fig. 8b). Analysis of the data in terms of Eq. (3) is not applicable as the SLD of the solvent no longer matches the SLD of the gold fronting layer and therefore the data is only interpreted via the least-squares fitting procedure. For the organic film, the differences between fits performed using fixed and floating parameters for Cr and Au layers were within experimental errors. However, the changes in the thickness and SLD of the Cr and Au layers were more pronounced. At the solid liquid interface, charging of a thin film of gold creates a significant surface stress [50,51]. The stress may affect the structure of the Cr and Au layers and in order to allow for such a change it is safe to allow the parameters of Cr and Au films to vary. For this reason, in the remaining section of this paper we will only discuss the data obtained using the second fitting

procedure (i.e. the SLD and thickness of Cr and Au layers were allowed to vary).

Table 3 lists the evaluated best-fit parameters for these two experiments. For $E = 100$ mV, reflectivities with very good statistics were measured out to $Q_z = 0.18$ Å^{-1} despite the higher background arising from the greater incoherent scattering of H_2O compared to D_2O. The best-fit model for the measurement at $E = 100$ mV gives a thickness for the d-C15-4Py film equal to 18 ± 3 Å and an SLD for the organic layer equal to $(5.65 \pm 0.4) \times 10^{-6}$ Å^{-2}. The thickness is consistent with the measurements performed on crystal 'C' with hydrogenated (h-C15-4Py). Again, the water content can be estimated using a modified version of Eq. (4). The SLD of H_2O is equal to -0.56×10^{-6} Å^{-2} while the SLD for the organic film is determined based on the density of per-deuterated alkanes and gives a value of $(6.6 \times 10^{-6}$ Å$^{-2})$. The water content is determined to be $(13 \pm 3)\%$. This well-formed monolayer agrees quite closely with the experiment performed at $+100$ mV with the GCMW contrast.

By going to a potential equivalent to cathodic desorption (-800 mV) one observes a pronounced increase in the thickness of the organic film ($\sim 18–34$ Å) and a change in the SLD indicating more than 38% of the volume is occupied by solvent. Again, these results are in good agreement to the model determined for the GCMW system. We wished to test the hypothesis that surfactant molecules are concentrated in the middle of the film and the region adjacent to the metal is water rich. We introduced an interstitial layer of solvent between the gold and the surfactant layer in our model of the interface. When the fitting routine was allowed to adjust this 'two-layer' model, the thickness of the water layer was driven to zero and the SLD of the outer layer became degenerate with the SLD determined for a one-layer model of the film. We note that fitting a model to the data for this potential gave the poorest fit in the whole series of measurements. A brief inspection of the data in Table 3 reveals the SLDs for the Cr and Au layers are significantly lower that the values for bulk metals. This behaviour suggests that, for crystal B, the gold film became porous when in contact with the electrolyte solution especially at the more negative electrode potential. The poorer quality fit for this substrate may therefore be related to poorer quality of Cr and Au coatings. Due to beam time restrictions we were not able to repeat this experiment using another substrate.

The last contrast experiments to discuss were performed on crystal 'A' using a monolayer film of hydrogenated C15-4Py and D_2O based electrolyte. The reflectivity measurements were conducted at $+100$, -300 and -750 mV vs SCE. Fig. 9a and b show the reflectivity curve for potentials $+100$ and -750 mV only. For -300 mV only the fit parameters are
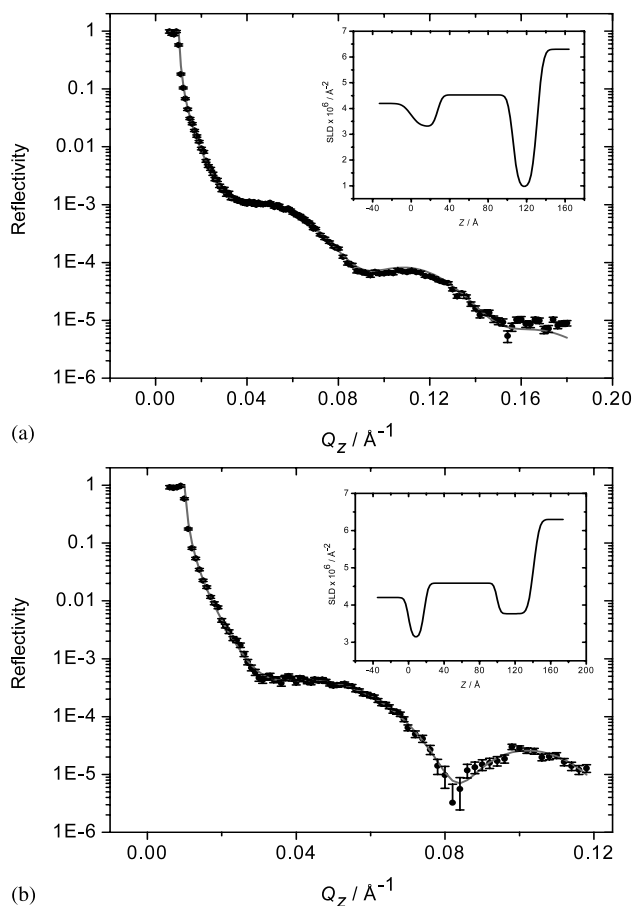

Fig. 9. Experimentally determined reflectivity curves (points with associated error bars) and calculated reflectivity curves (solid lines) from the best-fit modelling of hydrogenated C15-4Py (h-C15Py) measured against 50 mM NaF in D_2O. Panel A shows the data when the working electrode potential was 100 mV vs SCE and panel B for the measurement at $E = -850$ mV vs SCE. Insets to both panels provide the SLD profile of the interface in the direction perpendicular to the surface.

reported. The solid lines represent the reflectivity profile calculated from the best-fit model whose SLD profiles are depicted in the insets. The results of the fitting analysis for the hydrogenated C15-4Py monolayer in D_2O based electrolyte are shown in the last lines of Table 3. At 100 mV, the thickness of the layer between the gold and bulk electrolyte was 25 ± 2 Å and the SLD of this layer was determined to be $(0.87 \pm 0.1) \times 10^{-6}$ Å^{-2}. Using Eq. (4) the water content in the film is determined to be $(20 \pm 1)\%$. Evidently, the transfer of the C15-4Py molecules to the electrode interface from the air–solution interface was poorer for this experiment. As the determined thickness of the film matches the thickness for the previous experiments we assume that the poor transfer of surfactant left bare patches on the surface of the electrode leading to higher overall solvent content in the film. The reflectivity data for a patchy adsorbed layer at the interface can still be modeled and analyzed in terms of uniformly stratified media as long

as the area of the patches is smaller than the transverse coherence length of the neutrons. Otherwise, the analysis becomes very complicated see [52]. The neutron coherence length is the distance over which the neutron wavefront can be considered planar and for the range of Q_z values employed, it lies between 10 and 100 µm.

Changing the potential from 100 to −300 mV causes a slight increase in the water content. This behaviour is consistent with formation of pores in the film that leads to poorer barrier properties [24] and with a change in the conformation of the alkyl tails observed in recent IRRAS studies [28]. The best-fit model for the reflectivity measured at a potential of −750 mV suffers from weak reflectivity at Q_z greater than ~ 0.12 Å^{-1}. The drop in the reflectivity is qualitatively explained in terms of a drop in the contrast between the SLD of the adsorbed layer with the SLD of its fronting (gold) and its backing (the D$_2$O based electrolyte). Consistent with this observation, the fit reveals that the SLD of the layer adsorbed on the surface has increased to $(3.76 \pm 0.2) \times 10^{-6}$ Å^{-2}. With the help of Eq. (4), the water content in the film at −750 mV is (62 ± 3)%, three times of the water content at 100 mV. Despite the poorer signal of the reflectivity curve when $E = -750$ mV the fitting results are consistent with the analogous measurements for the two other contrasts.

4. Discussion and conclusions

We have employed NR to study the structure of a film formed by C15-4Py molecules at gold electrode surfaces using three different contrast systems. For all three contrasts the thickness of the surfactant film at $E = +100$ mV is on the order of 20 Å and is comparable to the length of a fully extended *all trans* C15-4Py molecule [20], indicating that the film consists of a monolayer of vertically oriented molecules with rather fully elongated alkyl tails. In terms of solvent content, the results for the d-C15Py in H$_2$O based electrolyte system agree very well with the results for the monolayer of hydrogenated C15Py in an electrolyte contrast matched to gold. Both films contain few defects as indicated by the low quantity of solvent in the organic layers. In comparison, the monolayer of hydrogenated C15Py measured against D$_2$O shows much greater amounts of solvent in the film formed at $E = 100$ mV. This is not unexpected result since we have already reported earlier [20] that the minimum differential capacity for a monolayer of C15-4Py deposited at a Au electrode surface may vary between 8 and 4 µF cm^{-2} depending on the efficiency of the transfer.

The differential capacity may be expressed as follows:

$$C = \frac{\varepsilon}{\tau} \tag{5}$$

where ε is the permittivity and τ is the thickness of the adsorbed layer. For a perfectly condensed monolayer film of C15-4Py, one can assume that $\tau \approx 20$ Å and that the permittivity is equal to the product of the permittivity of vacuum (8.85×10^{-12} F m^{-1}) and the square of the refractive index of a fully hydrogenated species (~ 1.4). These numbers give a minimum calculated capacitance for a monolayer equal to ≈ 1 µF cm^{-2}. At $E = 100$ mV the capacity of the film free interface is equal to ~ 35 µF cm^{-2}. With the help of the formula:

$$\theta = \frac{C_0 - C_{\text{film}}}{C_0 - C_1} \tag{6}$$

one may calculate the fraction of the electrode surface covered by the C15-4Py molecules. In Eq. (6), C_0 is the capacity of the film free interface and is equal to 35 µF cm^{-2}); C_1 (equal to 1 µF cm^{-2}) is the capacity of the electrode covered by the film and C_{film} is the experimentally observed capacity of the film covered electrode the value of which varies between 8 and 5 µF cm^{-2}. The higher value of C_{film} gives a film of 79% and the lower value yields 88% coverage. These numbers correspond to water contents of 21 and 12%, respectively, which are comparable to the water content in the films transferred onto the gold-coated quartz crystal in this work.

We would like to emphasize that Eq. (6) is approximate and that capacity can provide only approximate information concerning the water content in the film. Eq. (5) shows that capacity depends on the ratio of the permittivity and the thickness. Therefore, one has to assume the thickness to calculate the permittivity (composition of the film) or vice versa. In contrast, with the help of NR we were able to determine the thickness and the composition of the film independently. This is an important information that has already been used to calculate the tilt angle of the alkyl chains and the orientation of pyridine moiety in the film from PM IRRAS data, recently [28].

The NR data at potentials corresponding to cathodic desorption (−800 or −750 mV) answer the question of where the surfactant aggregates are located with respect to the electrode surface. Cumulatively, our fits to the three measurements with different contrasts indicate that surfactants remain in a layer adjacent to the electrode surface that is on the order of 30 to 40 Å thick. The results did not indicate that a water layer is separating the molecular aggregates from the electrode surface at negative potentials. They show that at sufficiently negative potentials the film swells and that leads to a significant influx of water into the film.

This behaviour is consistent with the model of a potential controlled de-wetting of the electrode surface from a film of organic molecules proposed in [25]. The model predicts that the de-wetting involves fragmentation of the film into drop like aggregates. The contact angle between the aggregate and the gold surface increases, when the potential becomes more negative. Consequently, the film changes from having a lens-like appearance to a pear-like or 'wasp-nest' appearance. Images of such a potential controlled change in an organic layer deposited onto an electrode surface were shown by Ivosevic and Zutic [53]. The formation of these weakly attached aggregates ('wasp-nests'), would lead to an overall thicker but much more porous organic layer. In principle, NR can be used to determine the shape of such aggregates [54]. Therefore, we have performed simulations similar to the one described in [54]. These calculations indicate that in our case the reflectivity measurements would have to be carried out with a resolution of ~ 8 Å up to $Q_{z,max} \approx 0.4$ Å^{-1} to distinguish between various shapes of the aggregates. The resolution of our measurements was insufficient to determine the fine structure of this film. However, recent methodological advances [12] indicate that such measurements should be possible in the near future.

We have demonstrated that NR can provide unique information concerning the water content and the thickness of an organic film at an electrode surface. In addition, we have shown that NR should be the technique of choice when one needs to determine the location of surfactant molecules desorbed from the electrode surface, at negative potentials. NR is a relatively new technique that electrochemists should add to the repertoire of 'nontraditional methods' used to study organic films at electrode surfaces.

Acknowledgements

References

[1] X. Sun, E. Bouchaud, A. Lapp, B. Farnoux, M. Daoud, G. Jannik, Europhys. Lett. 6 (1988) 207.

[2] J.E. Bradley, M. Lee, R.K. Thomas, A.J. Willat, J. Penfold, R.C. Ward, D.P. Gregory, W. Waschkowski, Langmuir 4 (1988) 821.

[3] T.M. Bayerl, R.K. Thomas, J. Penfold, A. Rennie, E. Sackmann, Biophys. J. 57 (1990) 1095.

[4] A.R. Rennie, E.M. Lee, E.A. Simister, R.K. Thomas, Langmuir 6 (1990) 1031.

[5] G. Fragneto, J.R. Lu, D.C. McDermott, R.K. Thomas, A.R. Rennie, P.D. Gallagher, S.K. Satija, Langmuir 12 (1996) 477.

[6] S.J. Johnson, T.M. Bayerl, D.C. McDermott, G.W. Adam, A.R. Rennie, R.K. Thomas, E. Sackmann, Biophys. J. 59 (1991) 289.

[7] D. Vaknin, M. Als-Nielsen, M. Piepenstock, M. Losche, Biophys. J. 60 (1991) 1545.

[8] G. Fragneto, R.K. Thomas, A.R. Rennie, J. Penfold, Science 267 (1995) 657.

[9] B.W. Koenig, S. Kruger, W.J. Orts, C.F. Majkrzak, N.F. Berk, J.V. Silverton, K. Gawrisch, Langmuir 12 (1996) 1343.

[10] (a) J.Y. Wong, J. Majewski, M. Seitz, C.K. Park, J.N. Israelachvili, G.S. Smith, Biophys. J. 77 (1999) 1445;
(b) J. Majewski, J.Y. Wong, C.K. Park, M. Seitz, J.N. Israelachvili, G.S. Smith, Biophys. J. 75 (1998) 2363.

[11] C.F. Majkrzak, N.F. Berk, S. Kruger, J.A. Dura, M. Tarek, D. Tobias, C.W. Meuse, J. Woodward, A.L. Plant, Biophys. J. 79 (2000) 3330.

[12] S. Kruger, C.W. Meuse, C.F. Majkrzak, J.A. Dura, N.F. Berk, M. Tarek, A.L. Plant, Langmuir 17 (2001) 511.

[13] D.W. Wiesler, C.F. Majkrzak, Physica B 198 (1994) 181.

[14] Z. Tun, J.J. Noel, D.W. Shoesmith, Physica B 241–242 (1998) 1107.

[15] Z. Tun, J.J. Noel, D.W. Shoesmith, J. Electrochem. Soc. 146 (1999) 988.

[16] J.J. Noel, H.L. Jensen, Z. Tun, D.W. Shoesmith, Electrochem. Solid State Lett. 3 (2000) 473.

[17] A.R. Hillman, P.M. Saville, A. Glidle, R.M. Richardson, S.J. Roser, M.J. Swann, J.R.P. Webster, J. Am. Chem. Soc. 120 (1998) 12882.

[18] A. Glidle, L. Bailey, C.S. Hadyoon, A.R. Hillman, A. Jackson, K.S. Ryder, P.M. Saville, M.J. Swann, J.R.P. Webster, R.W. Wilson, J.M. Cooper, Anal. Chem. 73 (2001) 5596.

[19] A.R. Hillman, L. Bailey, A. Glide, J.M. Cooper, N. Gadegaard, J.R.P. Webster, J. Electroanal. Chem. 532 (2002) 269.

[20] V. Zamlynny, I. Burgess, G. Szymanski, J. Lipkowski, J. Majewski, G. Smith, S. Satija, R. Ivkov, Langmuir 16 (2000) 9861.

[21] I. Burgess, V. Zamlynny, G. Szymanski, J. Lipkowski, J. Majewski, G. Smith, S. Satija, R. Ivkov, Langmuir 17 (2001) 3355.

[22] I. Burgess, V. Zamlynny, G. Szymanski, M. Li, S. Horswell, J. Lipkowski, J. Majewski, S. Satija, Biophys. J. Submitted.

[23] J. Majewski, G.S. Smith, I. Burgess, V. Zamlynny, G. Szymanski, J. Lipkowski, S. Satija, Appl. Phys. A, 74 (2002) S364 Suppl. S.

[24] D. Bizzotto, A. McAlees, J. Lipkowski, R. McCrindle, Langmuir 11 (1995) 3243.

[25] D. Bizzotto, J. Lipkowski, Prog. Colloid Polym. Sci. 103 (1997) 201.

[26] D. Bizzotto, V. Zamlynny, I. Burgess, C.A. Jeffrey, H.-Q. Li, J. Rubinstein, Z. Galus, A. Nelson, B. Pettinger, A.R. Merill, J. Lipkowski, in: A. Wieckowski (Ed.), Interfacial Electrochemistry, Theory, Experiment and Applications, Marcel Dekker, New York, 1999.

[27] T. Sagara, V. Zamlynny, D. Bizzotto, A. McAlees, R. McCrindle, J. Lipkowski, Isr. J. Chem. 37 (1997) 197.

[28] V. Zamlynny, I. Zawisza, J. Lipkowski, Langmuir 19 (2003) 132.

[29] D. Bizzotto, B. Pettinger, Langmuir 15 (1999) 8309.

[30] J. Shepherd, Y. Yang, D. Bizzotto, J. Electroanal. Chem. 524–525 (2002) 54.

[31] Y. Yang, D. Bizzotto, J. Electroanal. Chem. 500 (2001) 408.

[32] (a) D. Bizzotto, A. Nelson, Langmuir 14 (1998) 6269;
(b) D.F. Yang, H. AlMazani, M. Morin, J. Phys. Chem. B 101 (1997) 1158.

[33] M. Byloos, H. Al-Mazani, M. Morin, J. Phys. Chem. B 103 (1999) 6554.

[34] S.S. Wong, M.D. Porter, J. Electroanal. Chem. 484 (2000) 135.

[35] S. Sotiropoulos, A. Avranas, N. Papadopoulous, Langmuir 13 (1997) 7230.

[36] (a) A. Avranas, N. Papadopoulous, D. Papoutsi, S. Sotiropoulos, Langmuir 16 (2000) 6043;
(b) F.T. Buonisegni, L. Becucci, M.R. Moncelli, R. Guidelli, J. Electroanal. Chem. 500 (2001) 395.

[37] F.T. Buonisegni, R. Herrero, M.R. Moncelli, J. Electroanal. Chem. 452 (1998) 33.

[38] M. Hepel, J. Electroanal. Chem. 509 (2001) 90.

[39] G. Parratt, Phys. Rev. 95 (1954) 359.

[40] W.H. Press, S.A. Teukolsky, W.T. Vetterling, B.P. Flannery, Numerical Recipes in C, Cambridge University Press, New York, 1992, pp. 656–706 (Chapter 15).

[41] R. Lu, E.M. Lee, R.K. Thomas, Acta Cryst. A52 (1996) 11.

[42] R.K. Thomas, Prog.Colloid Polym. Sci. 103 (1997) 216.

[43] J. Penfold, R.K. Thomas, J. Phys.: Condensed Matter 63 (1990) 1314.

[44] C.F. Majkrzak, J.F. Ankner, N.F. Berk, D. Gibbs, in: L.H. Bennett, R.E. Watson (Eds.), Magnetic Multilayers, World Scientific Publishing Co, New Jersey, 1994, pp. 299–354.

[45] C.F. Majkrzak, in: D.A. Neumann, T.P. Russell, B.J. Wuensch (Eds.), Neutron Scattering in Materials Science II, Materials Research Society Publisher, 1995, pp. 143–156.

[46] C.F. Majkrzak, Acta Physica Polonica A 96 (1999) 81.

[47] W.N. Hansen, J. Opt. Soc. Am. 58 (1968) 380.

[48] Available from: http://rrdjazz.nist.gov/resources/sldcalc.html: site maintained by the NIST Center for Neutron Research.

[49] J. Als-Nielsen, Z. Phys. B61 (1985) 411.

[50] H. Ibach, C.E. Bach, M. Giesen, A. Grossmann, Surf. Sci. 375 (1997) 107.

[51] H. Ibach, Surf. Sci. Rep. 29 (1997) 193.

[52] K.Y.C. Lee, J. Majewski, T. Kuhl, P. Howes, K. Kjaer, M. Lipp, A.J. Waring, J.A. Zasadzinski, G.S. Smith, Biophys. J. 81 (2001) 572.

[53] N. Ivosevic, V. Zutic, Langmuir 14 (1) (1998) 231.

[54] J.C. Schulz, G.G. Warr, W.A. Hamilton, P.D. Butler, J. Phys. Chem. 103 (1999) 11057.